Inorganic Chemistry

ARTICLE

pubs.acs.org/IC

Combined Theoretical and Mass Spectrometry Study of the Formation-Fragmentation of Small Polyoxomolybdates

Laia Vilà-Nadal,[†] Elizabeth F. Wilson,[‡] Haralampos N. Miras,[‡] Antonio Rodríguez-Fortea,[*,†] Leroy Cronin,[*,‡] and Josep M. Poblet[*,†]

[†]Departament de Química Física i Inorgànica, Universitat Rovira i Virgili, c/Marcel·lí Domingo s/n, 43007 Tarragona, Spain

[‡]School of Chemistry, The University of Glasgow, University Avenue, Glasgow G12 8QQ, Scotland, U.K.

Supporting Information

ABSTRACT: We investigate the assembly of small polyoxomolybdates using Car−Parrinello molecular dynamics simulations which show that there is an expansion of the coordination sphere of the Mo center from four to six in molybdate anions when the acidity of the solution is increased. With the help of complementary static density functional theory (DFT) calculations and electrospray ionization mass spectrometry experiments, we are able to postulate tentative mechanisms, with energy-cascade profiles, for the formation of the Lindqvist $[Mo_6O_{19}]^{2-}$ anion. Similar to the family of isopolytungstates, it can be proposed that the $[Mo_6O_{19}]^{2-}$ is formed by the aggregation of one molybdenum unit at a time; however, significant differences with respect to isopolytungstates are also found. The different behavior of chromates with respect to molybdates and tungstates is also considered.

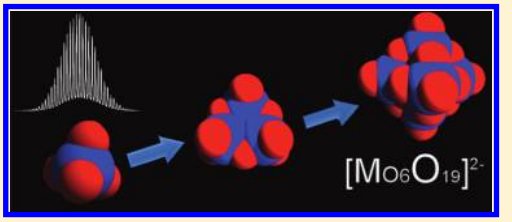

INTRODUCTION

If one considers all the transition metals, ranging from Sc to Hg, only few have the ability to form polymeric oxoanions. Indeed only vanadium, molybdenum, tungsten in high oxidation state, and, to a minor extent, niobium and tantalum can combine with oxygen to form polyoxometalates (POMs).[1a] Despite this restriction, POMs are represented by a vast and assorted group of compounds with significant chemical and physical properties.[1b] The first evidence of POMs dates back to Berzelius in the year 1826.[2] In recent decades research into polyoxometalate chemistry has grown exponentially and is still a developing area. Nuclearities can range from six metal atoms in the smallest clusters, up to 368 atoms reaching a size comparable to proteins.[3] Polyoxometalates present unique structural and electronic properties that make them attractive for applications in many fields.[4] For example, the ability of POMs to be reduced is well-known, so the applicability of this property has been used in catalysis, materials science, chemical analysis, and so forth.[5] Many attempts have been made to rationalize the structures of polyoxometalates. They can be classified with regard to their composition, the oxidation state of the metals, or their structural aspects. One of the most widely accepted classifications of POMs divides them in two groups: (i) isopolyanions (IPAs), which are oxides of only one type of M atom, $[M_mO_y]^{q-}$, and (ii) heteropolyanions (HPAs), with the formula $[X_rM_mO_y]^{q-}$, where X is the so-called heteroatom. In these generic formulas M is usually Mo or W, less frequently V, Nb, or Ta, or mixtures of these elements in their highest oxidation states (d^0, d^1). The heteroatom, X, can be a nonmetal, for example, P^V and Si^{IV} or a metal, for example, Co^{III} and Cu^I.

POMs are formed under experimental conditions that allow linking of polyhedra, that is, after acidification of alkaline aqueous solutions of simple oxoanions. Discrete structures are formed as long as the system is not driven to the oxide.[5] The polymerization of acidified solutions of Mo^{VI} or W^{VI} yields the most complicated of all the polyanion systems.[6] If these solutions are made strongly acidic, precipitates of yellow molybdenum oxide ($MoO_3 \cdot 2H_2O$) or white tungsten oxide ($WO_3 \cdot 2H_2O$) are obtained. The main limitation in the development of a universal polyoxometalate "lego" kit lies with the great sensitivity between synthetic conditions (pH, solvent, temperature, countercations) and the overall cluster architecture formed.[7]

Although extensive theoretical research has been performed in the area of POMs during past decades,[8] only a few studies have been devoted to study their formation mechanisms. Since the widely accepted bidentate mechanism suggested by Kepert[9] in the 1960s and the more elaborate mechanisms proposed by Tytko and Glemser[10] in the 1970s, there has been little advance in this area. Recent collaborative research carried out by Cronin, Poblet, and co-workers has helped to clarify the mechanism for the nucleation of the Lindqvist anion $[W_6O_{19}]^{2-}$.[11] Theoretical predictions combined with electrospray ionization mass spectrometry (ESI-MS) experiments have revealed themselves as important tools to understand such mechanisms. In this work, the mechanism for the formation of $[Mo_6O_{19}]^{2-}$ is discussed, and this is a continuation of previous work devised to shed light on the formation of low nuclearity iso- and heteroPOMs. To achieve

Received: May 9, 2011
Published: July 19, 2011

this goal, as in the case of $[W_6O_{19}]^{2-}$, we have performed ESI-MS experiments on $((n\text{-}C_4H_9)_4N)_2Mo_6O_{19}$[12] combined with complementary computational technique studies. Further, we have analyzed the formation-fragmentation mechanisms of the Lindqvist anion, $[Mo_6O_{19}]^{2-}$, focusing on the structures of the possible intermediate species. Before doing so, a study of the hydration of the monomeric building blocks $[MoO_3(OH)]^-$ under different pH conditions is also presented. Mononuclear six-coordinated molybdenum species such as $[MoO_3(H_2O)_3]$ or $[MoO_2(OH)(H_2O)_3]^+$ have been detected at molybdate concentrations lower than 10^{-4} M and low pH values.[13] The present analysis will show how the coordination number of the Mo atoms changes at different pH conditions.

EXPERIMENTAL SECTION

1. ESI-MS Experiments. *1.1. Synthesis.* The sample of $((n\text{-}C_4H_9)_4N)_2Mo_6O_{19}$ used in this study was synthesized using the procedure described previously.[14]

1.2. ESI-MS Solution Preparations. $((n\text{-}C_4H_9)_4N)_2Mo_6O_{19}$ Stock Solution: Into 5 mL of MeCN was dissolved 10 mg of $((n\text{-}C_4H_9)_4N)_2Mo_6O_{19}$. MS Dilution: An aliquot of 20 μL of $((n\text{-}C_4H_9)_4N)_2Mo_6O_{19}$ Stock Solution was made up to 4 mL with MeCN. We have done the experiment in MeCN because the TBA salt of the Lindqvist anion is not soluble in water. There are three main reasons to use TBA^+ as a cation for the Lindqvist anion instead of Na^+ or K^+. First, the TBA^+ cations have a much higher mass than Na^+ or K^+ and give a large separation between signals corresponding to differently charged or protonated cluster states. Second, the TBA^+ cations have a lower affinity than Na^+ or K^+ for the cluster anions and solvent molecules. Third, the use of MeCN can prevent clusters from decomposing, aggregating, or converting into other species, phenomena that are typically seen in aqueous solution. The experiment could be done in water; however, in addition to the previous considerations, highly complex and uninformative spectra are obtained. Such complex mass spectra are due to the rapid speciation of the clusters in aqueous solution and the various adducts formed with sodium or potassium cations (plus water ligands).

1.3. ESI-MS Experimental and Analyses. All MS data was collected using a Q-trap, time-of-flight MS (MicrOTOF-Q MS) instrument equipped with an electrospray (ESI) source supplied by Bruker Daltonics Ltd. The detector was a time-of-flight, microchannel plate detector, and all data was processed using the Bruker Daltonics Data Analysis 4.0 software, while simulated isotope patterns were investigated using Bruker Isotope Pattern software and Molecular Weight Calculator 6.45. The following parameters were consistent for all ESI-MS scans given below. The calibration solution used was Agilent ES tuning mix solution, Recorder No. G2421A, enabling calibration between approximately 100 m/z and 3000 m/z. This solution was diluted 60:1 with acetonitrile. Samples were introduced into the MS via direct injection at 180 μL/h. The electrospray source was used with the drying nitrogen gas temperature at approx +180 °C. The ion polarity for all MS scans recorded was negative, with the end plate offset at −500 V, funnel 1 RF at 300 Vpp, funnel 2 RF at 400 Vpp, and hexapole RF at 400 Vpp. The collision cell was filled with argon collision gas. Other MS parameters, and CID (also referred to as MS/MS(MRM), that is, MS/MS multiple reaction monitoring) parameters, which are set to specific values for each scan, are given in the Supporting Information. All theoretical peak assignments were determined via comparison of the experimentally determined isotopic patterns for each peak, with simulated isotopic patterns.

2. Computational Methodology. The calculations in the present work have been performed using density functional theory (DFT) methodology with the program package ADF (*Amsterdam Density Functional*).[15] The gradient-corrected functionals of Becke[16] and Perdew[17] for the exchange and correlation energies, respectively, were used to improve the description of the electronic density provided by the local density.[18] The valence electrons for all atoms were described with Slater-type basis functions of triple-ζ + polarization quality. The inner electrons have been kept frozen. Scalar relativistic corrections were included by means of the *zeroth-order regular approximation* (ZORA)[17] formalism. All the computed stationary points have closed-shell electronic structure. The present computational settings, BP86/TZP, have been demonstrated to be a satisfactory methodology for describing the electronic structure of polyoxometalates.[19] All the structures discussed through this work were fully optimized taking into account the solvent effects by means of a continuous model. We have used the Conductor-like Screening Model (COSMO)[20] as implemented in the ADF program package.[21] The ionic radii of the atoms, which define the dimensions of the cavity surrounding the molecule, are chosen to be 1.26 Å for Mo, 1.52 for O, and 1.20 for H. The dielectric constant (ε) is set to 78 so as to model water as solvent.

Regarding to the molecular dynamics (MD) simulations, they were performed at the DFT level by means of the CPMD program package.[22] The description of the electronic structure is based on the expansion of the valence electronic wave functions into a plane wave (PW) basis set, which is limited by an energy cutoff of 70 Ry. The interaction between the valence electrons and the ionic cores is treated through the pseudopotential (PP) approximation. Norm-conserving Martins-Troullier PPs are employed.[23] A semicore Mo PP was used according to the work of Boero et al.[24] We adopt the generalized gradient-corrected functionals of Becke for the exchange and of Perdew for the correlation.[16,17] In the MD simulations, the wave functions are propagated in the Car−Parrinello scheme, by integrating the equations of motion derived from the extended Car−Parrinello Lagrangian.[25] We use a time step of 0.144 fs and a fictitious electronic mass of 900 au. A Nosé-Hoover thermostat keeps the temperature around 300 K.[26] The cell box that contains (i) one $[MoO_3(OH)]^-$ and 29 H_2O molecules ($a = b = c = 9.959$ Å); (ii) two $[MoO_3(OH)]^-$ and 27 H_2O molecules ($a = b = c = 9.959$ Å); or (iii) three $[MoO_3(OH)]^-$ and 58 H_2O molecules ($a = b = c = 12.580$ Å) is repeated periodically in space by the standard periodic boundary conditions.

The limited simulation time affordable by standard MD runs does not allow the observation of rare events like thermally activated chemical reactions. For this reason, we employ the metadynamics technique, which is capable of efficiently reconstructing complex reaction mechanisms and provides the free energy profile, as demonstrated in previous applications.[27] A detailed description of the metadynamics method associated with Car−Parrinello MD can be found elsewhere.[28] The metadynamics simulations are based on the selection of collective variables (CV) that are suitable to describe the process. In this work, we often use as CV the coordination number (CN) of one atom, or group of atoms, A, with respect to a second atom, or group of atoms, B.[28b,29] The analytic definition of the CN of B with respect to A can be found elsewhere.[28b] In the present work, $p = 8$ and $q = 14$ are used. More details about the metadynamics simulations are found in the Supporting Information.

RESULTS AND DISCUSSION

1. Hydration of $[MoO_3(OH)]^-$ and $[MoO_2(OH)_2]$. We have studied the hydration-dehydration equilibria of the hydrogenmolybdate anion, $[MoO_3(OH)]^-$, and molybdic acid, $[MoO_2(OH)_2]$, including explicit solvent (water) molecules using Car−Parrinello MD and metadynamics simulations. First of all, the stability of $[MoO_3(OH)]^-$ and the corresponding mono-, $[MoO_3(OH)(H_2O)]^-$, and dihydrated species, $[MoO_3(OH)(H_2O)_2]^-$, is analyzed. The nonhydrated tetrahedral anion

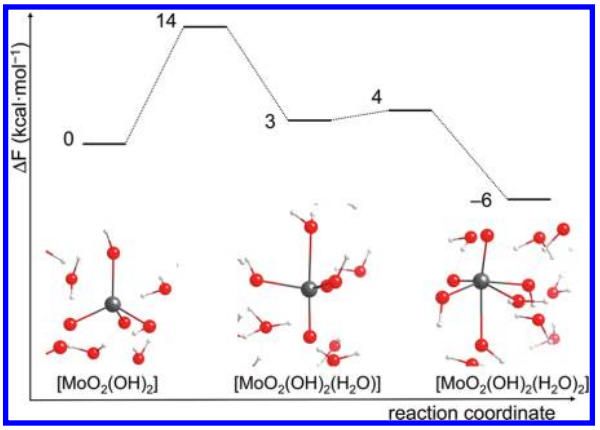

Figure 1. Free-energy profile (in kcal·mol^{-1}) corresponding to the hydration-dehydration equilibria of molybdic acid along with the ball-and-stick representation of the four-, $[MoO_2(OH)_2]$, five-, $[MoO_2(OH)_2(H_2O)]$, and six-coordinated, $[MoO_2(OH)_2(H_2O)_2]$, species.

is seen to be stable during the simulations, in good agreement with well accepted experimental data.[1] However, the five-coordinated monohydrated and the six-coordinated dihydrated species are not found to be stable, that is, the water molecules that were initially bound to the Mo^{VI} ion are rapidly released during standard Car−Parrinello MD simulations, especially the five-coordinated species, which is observed for less than 1 ps. Therefore, the hydrogenmolybdate anion retains the tetrahedral coordination for most of the time. The effect of the acidification of the solution on the hydration equilibria is also considered. To do so, we have analyzed the free-energy changes for the following equilibrium reactions (eqs 1 and 2),

$$[MoO_2(OH)_2] + H_2O \rightleftarrows [MoO_2(OH)_2(H_2O)] \quad (1)$$

$$[MoO_2(OH)_2(H_2O)] + H_2O \rightleftarrows [MoO_2(OH)_2(H_2O)_2] \quad (2)$$

Molybdic acid is the predominant species when the pH of the solution is somewhat lower than $pK_{a,1} = 3.61$.[1] The computed free-energy profile, depicted in Figure 1, is obtained by averaging the results of several metadynamics simulations (see Supporting Information). The compound with the six-coordinated Mo^{VI} ion shows the lowest free energy, 9 and 6 kcal mol^{-1} lower than that observed for the five- and four-coordinated species, respectively. This is in contrast with the results observed at higher pH conditions (around $pK_{a,2} = 3.89$) with the hydrogenmolybdate anion.

Although the free-energy barrier for the formation of the six-coordinated species from the five-coordinated one is very small (1 kcal mol^{-1}), the barrier for the formation of the latter is far from being negligible (14 kcal mol^{-1}). However, we have to consider these 14 kcal mol^{-1} as an upper limit for the barrier because during the metadynamics simulation corresponding to this process (eq 1), deprotonation of the molybdic acid is observed prior to hydration. These results can be easily rationalized from a qualitative point of view: the Mo^{VI} ion is more electrophilic in the molybdic acid than in the hydrogenmolybdate anion and, therefore, it is more easily attacked and stabilized by the nucleophilic water molecules. Therefore, in agreement with what is observed for mononuclear tungstate species,[27a] a decrease of the pH of the aqueous solution involves an *expansion* of the coordination sphere of the Mo^{VI} ion, as proposed from previously reported experimental data.[1]

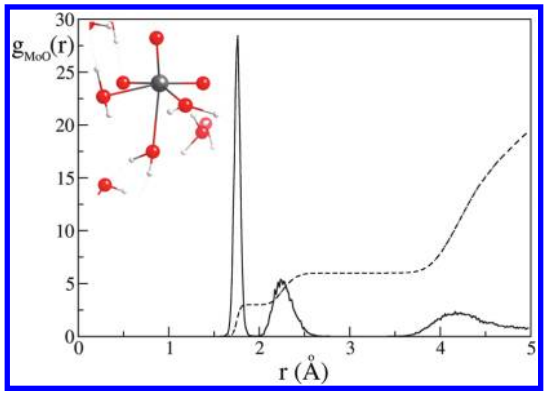

Figure 2. Mo−O radial distribution function (solid line) and its integration (broken line) for the 28 ps MD simulation starting from $[MoO_3(H_2O)_3]$. The ball-and-stick representation of the hydrated monomer is shown at the top left corner.

We have also examined the stability at low pH conditions ($pH < pK_{a,1} = 3.61$) of two structural isomers of six-coordinated molybdic acid, $[MoO_2(OH)_2(H_2O)_2]$ and $[MoO_3(H_2O)_3]$. From standard Car−Parrinello MD simulations, we have observed that the two structural isomers are stable for 28 ps, that is, both of them remain as six-coordinated species (see below and Supporting Information). The Mo−O radial distribution function for $[MoO_3(H_2O)_3]$ and its integration, which yields the Mo−O coordination number, are displayed in Figure 2 (see Supporting Information for $[MoO_2(OH)_2(H_2O)_2]$).

The sharp spike below 2 Å, which integrates three O atoms, is attributed to the oxo ligands. The spike between 2 and 2.6 Å, which integrates three other O atoms, is due to the aqua ligands coordinated to the Mo^{VI} ion. At distances between 2.6 and 3.7 Å, the Mo−O coordination number shows a plateau associated with the presence of six O atoms in the coordination sphere of the Mo^{VI} ion. The shallow maximum that appears at around 4 Å and that does not fall to zero above 4.5 Å is associated to the first solvation shell of $[MoO_3(H_2O)_3]$ and the exchange of water molecules between this shell and the bulk solvent. Therefore, the structural isomers derived from hydrated molybdic acid, with Mo^{VI} ions featuring expanded coordination spheres, are shown to be stable at low molybdate concentrations and low pH conditions ($pH < pK_{a,1}$).

2. Formation of Dinuclear Clusters. Car−Parrinello MD simulations were also performed to study the first step of the growth mechanism at slightly acidic pH conditions (pH around $pK_{a,2}$), that is, the formation of dinuclear $[Mo_2O_6(OH)_2]^{2-}$ species from the $[MoO_3(OH)]^-$ building blocks. The metadynamics approach was used to accelerate the dynamics and to compute the free-energy profile. The system was formed by 2 $[MoO_3(OH)]^-$ monomers and 27 H_2O molecules. To describe the formation of dinuclear species several metadynamics runs were performed, all of them using, as collective variables (CV), the coordination number (CN) of each Mo atom with respect to the eight O atoms from the MoO_4 groups, C_{Mo1-O} and C_{Mo2-O} (see Supporting Information). Several common events are observed in the different simulations. First, formation of a dinuclear species in which one Mo^{VI} ion is five-coordinated and the other is four-coordinated (a 5c-4c structure, see Figure 3) is observed. After some picoseconds (ps), a recrossing to reactants takes place, that is, the dimolybdate is broken yielding the two original hydrogenmolybdate anions. These dimerization and

dx.doi.org/10.1021/ic200969h |*Inorg. Chem.* 2011, 50, 7811–7819

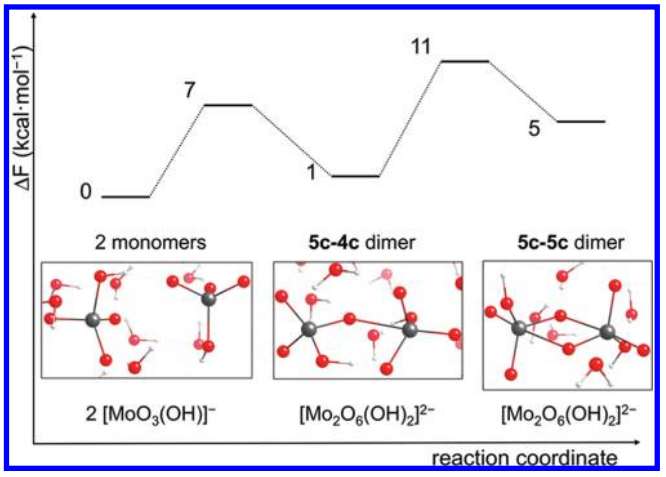

Figure 3. Free-energy profile (in kcal mol^{-1}) corresponding to the formation of dinuclear $[Mo_2O_6(OH)_2]^{2-}$ species along with the ball-and-stick representation of the three observed minima: the 2 monomers, the 5c-4c dimer, and the 5c-5c dimer.

Table 1. Reaction Energies for Di- and Trinuclear Mo Species with Respect to Two Monomers Using the COSMO Methodology[a,b,c,d]

stoichiometry	structure	type	Cr	Mo	W
$[M_2O_6(OH)_2]^{2-}$	**di-1**	5c-4c	+17.0	+0.4	−7.4
	di-2	5c-5c	diss[e]	+7.4	+0.2
	di-3	5c-5c	diss[e]	+11.4	+10.2
$[M_2O_7]^{2-}$	**di-4**	4c-4c	−2.7	−2.2	−5.3
$[M_3O_{10}(OH)]^{3-}$	**tr-1**		+33.4	+7.8	−3.7

[a] The values for M = Cr and W are also provided for comparison. [b] In kcal mol^{-1}. [c] For $[M_3O_{10}(OH)]^{3-}$, reaction energy with respect to $[M_2O_7]^{2-}$ and $[MO_3(OH)]^-$. [d] The values for M = W are from ref 11. [e] The optimization leads to dissociation into the monomers.

recrossing steps recur for a time before finally the 5c-5c structure is obtained (Figure 3). During the simulation H^+-transfers between (i) the monomers, (ii) the solvent molecules, and (iii) the molybdates and the solvent molecules are also frequent. Thus, these events, which have not been accelerated by the metadynamics must have small free-energy barriers, that is, they are highly likely. Two other points are also interesting to mention here. The first is that, in contrast to dinuclear tungstates,[11,30] no expansion of the coordination sphere of the Mo^{VI} ions is observed at this pH because of coordination of the solvent water molecules, in good agreement with the previous results on hydrogenmolybdate anions. The second is that the 6c-4c structure proposed by Kepert for the first aggregation step was not observed in these simulations. Hence, this type of dimer, if it exists, must have a higher formation barrier than the 5c-4c and 5c-5c structures.

The free-energy profile (Figure 3) shows that formation of the 5c-4c structure requires a barrier of only 7 ± 1 kcal mol^{-1}. The barrier for breaking the 5c-4c dimer is smaller than that for the formation of the 5c-5c structure (6 vs 10 kcal mol^{-1}). All these barriers are, however, easily overcome at the temperature at which POMs are formed. Regarding the relative free energies of the minima, the formation of the 5c-5c structure is clearly endergonic

Figure 4. Lowest-energy structures at BP86/COSMO level for dinuclear clusters with $[M_2O_6(OH)_2]^{2-}$ and $[M_2O_7]^{2-}$ stoichiometries.

(5 kcal mol^{-1}), whereas the 5c-4c structure shows a free-energy similar to that of the two monomers (1 kcal mol^{-1}).

Reaction energies for dinuclear species with respect to the two hydrogenmolybdate anions (eq 3) using the COSMO method to account for the solvation effects are listed in Table 1.

$$2[MoO_3(OH)]^- \rightarrow [Mo_2O_6(OH)_2]^{2-} \quad (3)$$

$$2[MoO_3(OH)]^- \rightarrow [Mo_2O_7]^{2-} + H_2O \quad (4)$$

The lowest-energy minimum for the $[Mo_2O_6(OH)_2]^{2-}$ stoichiometry corresponds to the **di-1** structure of 5c-4c type, which is at least 7 kcal mol^{-1} more stable than the other structures of 5c-5c type (**di-2** and **di-3**), see Figure 4. The formation of these dimers is predicted to be endothermic in all cases. The difference between the two 5c-5c structures is that in **di-2** the H atoms are located at the terminal O atoms, whereas in **di-3** they are located at the bridge O atoms. The lower energy of **di-2** with respect to **di-3** indicates that terminal O atoms are more basic than those in bridging positions. This result is similar to that found for ditungstates,[30] but it is in contrast to the behavior observed for large POMs in which the bridging positions are those with the highest basicities.[31] The formation of the dehydrated dimer, $[Mo_2O_7]^{2-}$, with the **di-4** structure of 4c-4c type (see eq 4 and Figure 4), is somewhat exothermic (−2.2 kcal mol^{-1}). It is also interesting to point out that the structure of 6c-4c type proposed by Kepert has not been found as a minimum in the potential energy surface (PES) of $[Mo_2O_6(OH)_2]^{2-}$. All the geometry optimization attempts starting from a 6c-4c structure lead to 5c-5c structures.

We would also like to mention here the special case of chromates. This is because it is experimentally well-known that the behavior of Cr is very different from that of W or Mo. The Inorganic Chemistry textbooks teach that yellow solutions of chromate anions, $[CrO_4]^{2-}$, become orange when the pH of the solution is lowered because of the formation of stable dichromate anions, $[Cr_2O_7]^{2-}$, according to eq 5.[32] In general, no further nucleation is observed in acidic solutions in contrast to the behavior found for tungstates or molybdates.

$$2[CrO_4]^{2-} + 2H_3O^+ \rightarrow [Cr_2O_7]^{2-} + 3H_2O \quad (5)$$

The reaction energies for the three structural isomers of $[Cr_2O_6(OH)_2]^{2-}$ and for the lowest-energy structure of $[Cr_3O_{10}(OH)]^{3-}$ are displayed in Table 1. The formation of the dehydrated dichromate anion, $[Cr_2O_7]^{2-}$, is much more favorable

dx.doi.org/10.1021/ic200969h |*Inorg. Chem.* 2011, 50, 7811–7819

Table 2. Proposed Mechanism (M1) for the Formation of the Lindqvist Anion $[Mo_6O_{19}]^{2-}$ [a,b,c]

step	transformation	RE	process type
1	$[MoO_3(OH)]^-_{(aq)} + [MoO_3(OH)]^-_{(aq)} \rightarrow [Mo_2O_6(OH)_2]^{2-}_{(aq)}$ (di-1)	+0.4	aggregation
2	$[Mo_2O_6(OH)_2]^{2-}_{(aq)} \rightarrow [\mathbf{Mo_2O_7}]^{2-}_{(aq)}$ (di-4) + $H_2O_{(aq)}$	−2.7	water condensation
3	$[Mo_2O_7]^{2-}_{(aq)} + [MoO_3(OH)]^-_{(aq)} \rightarrow [Mo_3O_{10}(OH)]^{3-}_{(aq)}$ (tr-1)	+7.8	aggregation
4	$[Mo_3O_{10}(OH)]^{3-}_{(aq)} + H_3O^+_{(aq)} \rightarrow [\mathbf{Mo_3O_{10}}]^{2-}_{(aq)}$ (tr-5) + $2H_2O_{(aq)}$	−11.0	water condensation
5	$[Mo_3O_{10}]^{2-}_{(aq)} + [MoO_3(OH)]^-_{(aq)} \rightarrow [Mo_4O_{13}(OH)]^{3-}_{(aq)}$ (te-2)	−9.6	aggregation
6	$[Mo_4O_{13}(OH)]^{3-}_{(aq)} + H_3O^+_{(aq)} \rightarrow [\mathbf{Mo_4O_{13}}]^{2-}_{(aq)}$ (te-4) + $2H_2O_{(aq)}$	−21.7	water condensation
7	$[Mo_4O_{13}]^{2-}_{(aq)} + [MoO_3(OH)]^-_{(aq)} \rightarrow [Mo_5O_{16}(OH)]^{3-}_{(aq)}$ (pe-1)	+9.3	aggregation
8	$[Mo_5O_{16}(OH)]^{3-}_{(aq)} + H_3O^+_{(aq)} \rightarrow [\mathbf{Mo_5O_{16}}]^{2-}_{(aq)}$ (pe-4) + $2H_2O_{(aq)}$	−1.2	water condensation
9	$[Mo_5O_{16}]^{2-}_{(aq)} + [MoO_3(OH)]^-_{(aq)} \rightarrow [Mo_6O_{19}(OH)]^{3-}_{(aq)}$ (he-1)	−7.2	aggregation
10	$[Mo_6O_{19}(OH)]^{3-}_{(aq)} + H_3O^+_{(aq)} \rightarrow [\mathbf{Mo_6O_{19}}]^{2-}_{(aq)}$ (he-2) + $2H_2O_{(aq)}$	−31.8	water condensation

[a] Reaction energies (RE) are in kcal mol^{-1}. [b] The species detected in the ESI-MS experiments are highlighted in bold. [c] In parentheses, the structures that are used to compute the reaction energies.

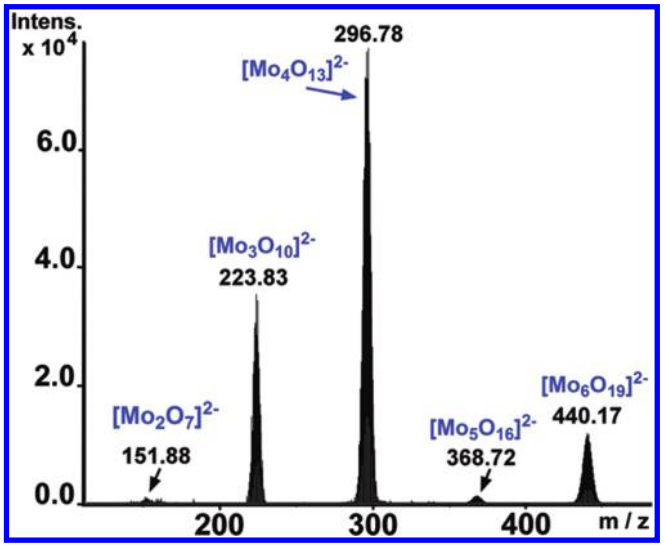

Figure 5. Mass spectral data recorded by collision induced dissociation (CID) of the isolated $[Mo_6O_{19}]^{2-}$ peak at m/z 440.17 (see the Supporting Information for more details). The fragment peaks shown are associated with the species $[Mo_2O_7]^{2-}$ (m/z 151.88), $[Mo_3O_{10}]^{2-}$ (m/z 223.83), $[Mo_4O_{13}]^{2-}$ (m/z 296.78), and $[Mo_5O_{16}]^{2-}$ (m/z 368.72).

(20 kcal mol^{-1}) than the formation of the $[Cr_2O_6(OH)_2]^{2-}$ dimer, indicating the preference of Cr^{VI} ions for *tetrahedral* coordination. Moreover, only the 5c-4c structure (**di-1**) is stable for $[Cr_2O_6(OH)_2]^{2-}$ stoichiometry whereas the others of 5c-5c type dissociate into the monomers. The formation of the trinuclear species $[Cr_3O_{10}(OH)]^{3-}$, predicted to be a highly endothermic process, can explain the fact that polyoxochromates with higher nuclearities are much less abundant than polyoxotungstates and molybdates.

3. From Trinuclear Species to the Lindqvist Anion: Combining Theory and ESI-MS Results. On the basis of consecutive steps of nucleation and water condensation, tentative mechanisms for the formation of the Lindqvist anion, $[Mo_6O_{19}]^{2-}$, consistent with the ESI-MS experiments, are put forward (Table 2). Even though fragmentation experiments give insight into the favored decomposition pathways of gas-phase clusters, they may also provide hints on potential intermediates that help to better understand the thermal assembly of POMs cluster anions. The peaks observed in the ESI-MS experiments (Supporting Information, Table S2 and Figure 5) are associated with the species $[Mo_2O_7]^{2-}$, $[Mo_3O_{10}]^{2-}$, $[Mo_4O_{13}]^{2-}$, $[Mo_5O_{16}]^{2-}$, and $[Mo_6O_{19}]^{2-}$.

The observed set of peaks belong to the previously observed group of species with the general formula $[Mo_mO_{3m+1}]^{2-}$ and in agreement with the studies of Walanda, von Nagi-Felsobuki et al.[32] and Llusar, Vicent et al.[33] In this case, we did not detect any species of the protonated set with the general formula $[HMo_mO_{3m+1}]^-$ since their formation depends greatly upon the solvent composition (aqueous and protic acidified media) and application of harsher ionization conditions (high collision energy values).[32,33] Consequently, the use of acetonitrile solution and application of mild ionization conditions during the course of our fragmentation experiments led only to the formation of the nonprotonated set, $[Mo_mO_{3m+1}]^{2-}$, of species in the gas phase.

Even though the peaks for the $[Mo_mO_{3m}(OH)]^-$ stoichiometries (m = 2 to 6) were not observed in the mass spectra, we have also proposed a mechanism that involves such species in analogy with previous studies in isopolytungstates (see Supporting Information for the alternative mechanism, M2).[11] For each of the stoichiometries observed in the ESI-MS spectra, a search for the lowest-energy structure in solution was carried out using the COSMO methodology. Geometry optimizations in the gas phase were also done for some clusters.

The dinuclear species with $[Mo_2O_6(OH)_2]^{2-}$ stoichiometry, which are formed in the first step of nucleation, should undergo dehydration to $[Mo_2O_7]^{2-}$ to be consistent with the ESI-MS results. Aggregation of a hydrogenmolybdate anion to $[Mo_2O_7]^{2-}$ leads to the formation of $[Mo_3O_{10}(OH)]^{3-}$ (step 3, Table 2). Relative energies and geometries for representative structural isomers of $[Mo_3O_{10}(OH)]^{3-}$ and $[Mo_3O_{10}]^{2-}$ are presented in Table 3 and Figure 6. The structures corresponding to stoichiometries derived from the alternative mechanism, which differ only in one H^+, are very similar to the ones shown here (see Supporting Information). The lowest-energy structure for the $[Mo_3O_{10}(OH)]^{3-}$ stoichiometry, **tr-1**, is a compact and planar μ_3-O trinuclear cluster which shows slightly lower energies than those with more open frameworks (Table 3). This structure was also found to have the lowest energy for the trinuclear $[W_3O_{10}(OH)]^{3-}$ isopolytungstates.[11]

Regarding the $[Mo_3O_{10}]^{2-}$ stoichiometry, the lowest-energy structure corresponds to an open cluster in which the three Mo^{VI} ions show tetrahedral coordination, that is, a chain of corner-

Table 3. Relative Energies (ΔE) for the Optimized Structures (COSMO Method) of Some Representative Tri-, Tetra- and Pentanuclear Species[a]

stoichiometry	structure	O coordination[b]	ΔE
$[Mo_3O_{10}(OH)]^{3-}$	**tr-1**	3	0.0
	tr-2	2	0.5
$[Mo_3O_{10}]^{2-}$	**tr-3**	2	−19.4
	tr-4	2	−4.0
	tr-5	3	0.0
$[Mo_4O_{13}(OH)]^{3-}$	**te-1**	2	−1.1
	te-2	3	0.0
	te-3	3	5.5
$[Mo_4O_{13}]^{2-}$	**te-4**	3	0.0
	te-5	4	3.9
$[Mo_5O_{16}(OH)]^{3-}$	**pe-1**	3	0.0
	pe-2	4	3.4
$[Mo_5O_{16}]^{2-}$	**pe-3**	3	−1.0
	pe-4	5	0.0

[a] The energies, in kcal mol^{-1}, are relative to the lowest-energy compact isomer for each stoichiometry. [b] Highest coordination of an O atom within the cluster.

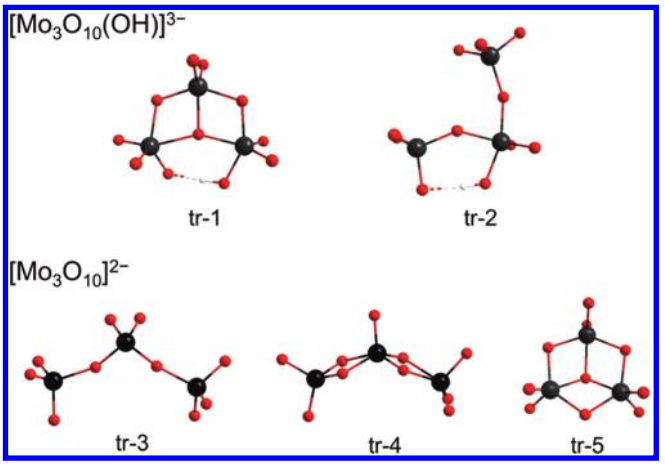

Figure 6. Ball-and-stick representations for the optimized structures of the most representative trinuclear species with $[Mo_3O_{10}(OH)]^{3-}$ (**tr-1** and **tr-2**) and $[Mo_3O_{10}]^{2-}$ (**tr-3**, **tr-4** and **tr-5**) stoichiometries.

sharing tetrahedra (**tr-3**, Figure 6). These type of structures were proposed by Walanda et al. as intermediates for an open-chain addition polymerization mechanism that might explain the formation of isopolymolybdates in the charged droplets formed in the ESI-MS experiments.[32] An open-chain cluster with one five- and two four-coordinated Mo^{VI} ions (**tr-4**) and one close-compact structure with a central tricoordinated O atom, μ_3-O, (**tr-5**) show much larger energies. The trinuclear open-chain structure **tr-3** is also much more stable than the compact isomer **tr-5** in the gas phase (19 kcal mol^{-1}). So, this open-chain **tr-3** isomer is probably the structure for the species detected with m/z peak of 223.83 in the spectrometer.

At this point, the following question arises: Is this trinuclear open-chain structure one of the intermediates in the formation of the Lindqvist anion? To check the stability of such trinuclear **tr-3** structure in solution, a 13-ps standard Car−Parrinello MD for the system formed by one open-chain $[Mo_3O_{10}]^{2-}$ cluster and

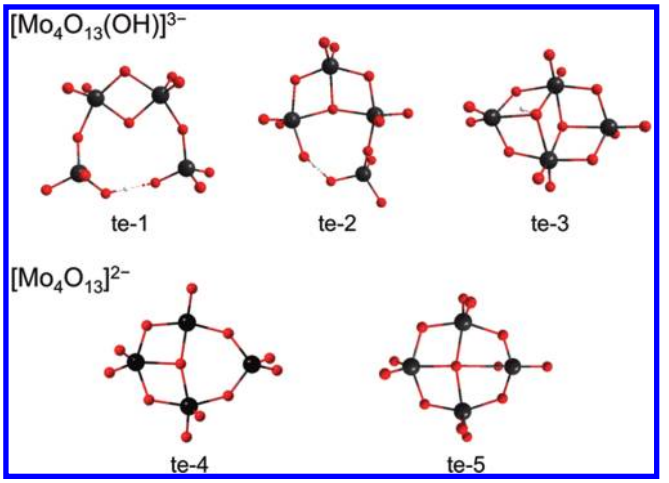

Figure 7. Ball-and-stick representations for the optimized structures of the most representative tetranuclear species with $[Mo_4O_{13}(OH)]^{3-}$ (**te-1**, **te-2**, and **te-3**) and $[Mo_4O_{13}]^{2-}$ (**te-4** and **te-5**) stoichiometries.

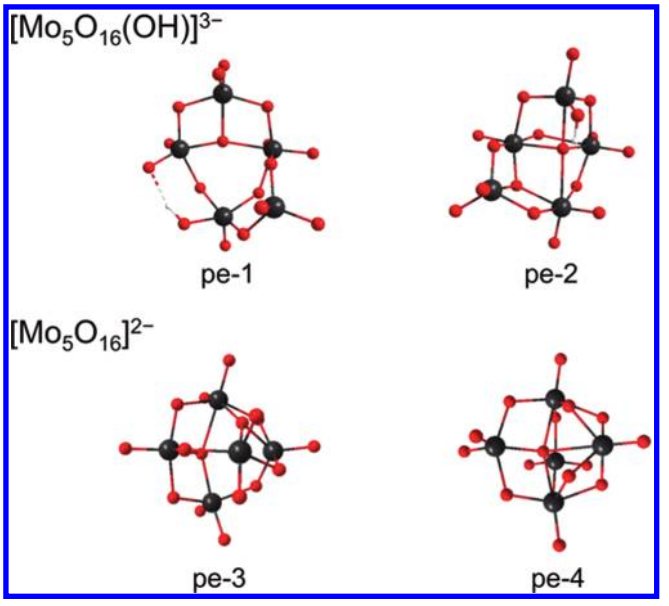

Figure 8. Ball-and-stick representations for the optimized structures of the most representative pentanuclear species with $[Mo_5O_{16}(OH)]^{3-}$ (**pe-1**, **pe-2**) and $[Mo_5O_{16}]^{2-}$ (**pe-3** and **pe-4**) stoichiometries.

58 H_2O molecules was performed. Analyses of the trajectory as well as the Mo−O radial distribution function for each of the Mo^{VI} ions (see Supporting Information) show that some H_2O molecules interact with the Mo^{VI} ions, especially with the central one. In fact, an expansion to octahedral coordination takes place for this central Mo^{VI} ion. Terminal Mo^{VI}, which retain their initial tetrahedral coordination, remain singly bonded to the central octahedron maintaining the original open structure. It is interesting to point out that the central Mo^{VI} ion is predicted to be the most electrophilic among the three metal ions (see Supporting Information). Thus, the most electrophilic Mo^{VI} ions might expand their coordination sphere because of the water molecules or the nucleophilic solvent.

Therefore, the $[Mo_3O_{10}(H_2O)_2]^{2-}$ open structure is found to be stable in solution, but it seems more feasible from a mechanistic point of view that other more compact structures derived from

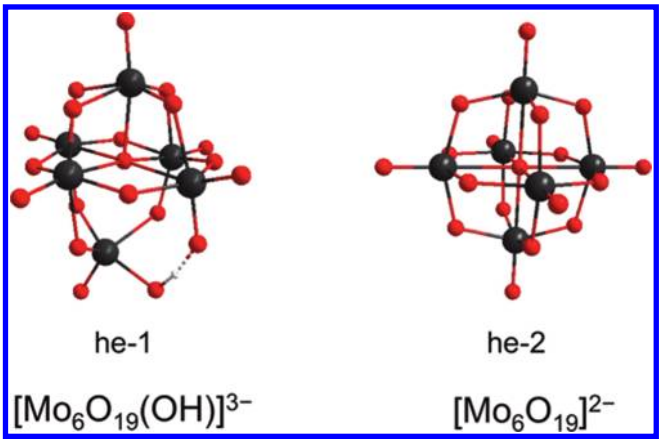

Figure 9. Ball-and-stick representations for the optimized structures corresponding to $[Mo_6O_{19}(OH)]^{3-}$ stoichiometry and the Lindqvist anion $[Mo_6O_{19}]^{2-}$.

the **tr-1** structure, as for example **tr-5**, could be the real intermediates that form the Lindqvist anion. For this reason, we have chosen the energies of such compact structures to compute the reaction energies in the mechanism shown in Table 2.

The lowest-energy structure that we found for $[Mo_4O_{13}(OH)]^{3-}$ stoichiometry, **te-1**, resembles that of a 5c-5c dimer with two extra corner-shared tetrahedral MoO_4 units (Figure 7). A more compact structure with the planar trinuclear motif and an extra corner-shared monomer, **te-2**, is almost quasidegenerate with **te-1** (1.1 kcal mol^{-1}). We have chosen this **te-2** structure to compute the reaction energies in the mechanism of Table 2. Structure **te-3**, with two μ_3-O atoms, is more compact and symmetric than the others, but it appears to have a higher energy (5 kcal mol^{-1}, Table 3). For $[Mo_4O_{13}]^{2-}$, the lowest-energy structure among those that we have computed, **te-4**, corresponds to a compact cluster where a trinuclear planar motif with a 3-fold coordinated O atom (μ_3-O) can be identified (see Table 3 and Figure 7). A similar compact structure with a μ_4-O atom, **te-5**, shows a somewhat higher energy (3.9 kcal mol^{-1}). The open-chain linear cluster with four corner-sharing tetrahedral Mo^{VI} ions lies only 1.3 kcal mol^{-1} higher in energy than **te-4** (5.4 kcal mol^{-1} in the gas phase). Although we have not performed Car−Parrinello MD simulations to analyze the behavior of such open structure in solution because of their high computational cost, we can state that some of the four Mo^{VI} ions will expand their coordination sphere in solution as observed for the trinuclear linear cluster.

The structures with the lowest energies for $[Mo_5O_{16}(OH)]^{3-}$ are depicted in Figure 8. Similarly to the previous case, the most compact structure **pe-2** with a μ_4-O atom shows a somewhat higher energy (3.4 kcal mol^{-1}, Table 3) than structure **pe-1**, which has a stabilizing planar trinuclear motif. Regarding the $[Mo_5O_{16}]^{2-}$ stoichiometry, two compact structures are found to have very similar energies (Table 3, Figure 8). Structure **pe-4**, with a μ_5-O atom, shows a framework that is rather similar to that of the Lindqvist anion. An analogous structure was also proposed for the case of isopolytungstates.[11] Interestingly, the open-chain linear structures with five corner-shared tetrahedra are predicted to have much lower energies than these compact clusters **pe-3** and **pe-4** (around 10 and 30 kcal mol^{-1} in gas phase and water solution, respectively). The hexanuclear Lindqvist anion, however, is not formed from these open-chain pentanuclear linear structures, but from compact clusters as for example the **pe-4** structure. As in the case of the trinuclear clusters, these open-chain pentanuclear species might exist in the chamber of the spectrometer when doing the ESI-MS experiments (peak at m/z 368.72), but they are not likely intermediates in the formation of the Lindqvist anion in solution.

Finally, the same analysis was performed for hexanuclear species. In a similar manner to the study of the isopolytungstates,[11,30] only compact structures that resemble that of the Lindqvist anion are analyzed here. In Figure 9 one can observe a $[Mo_6O_{19}(OH)]^{3-}$ structure, **he-1**, which will lead to the Lindqvist anion, **he-2**, after a protonation and a dehydration. It is important to note that the open-chain $[Mo_6O_{19}]^{2-}$ structure with six corner-shared tetrahedra shows a much higher energy than the Lindqvist structure in the gas phase (around 30 kcal mol^{-1}); however, it is predicted to have a lower energy than the Lindqvist structure (−2.1 kcal mol^{-1}) when the solvent (water) is taken into account. As detailed in the Experimental Section, the $[Mo_6O_{19}]^{2-}$ anion is usually prepared in nonaqueous media (DMF or acetonitrile), but it was originally obtained by precipitation from acidified aqueous molybdate solution.[34] So, it seems that the COSMO methodology that we are using here is overstabilizing somewhat those linear compounds with corner-sharing Mo^{VI} tetrahedra with respect to compact edge-sharing Mo^{VI} octahedra. We would also like to remark here that, in contrast to the idea of Walanda et al., who suggested that close-packed clusters are generally associated with larger-sized highly negatively charged aggregates in the ESI-MS experiments, the compact Lindqvist structure is predicted to have much lower energy than the $[Mo_6O_{19}]^{2-}$ open-chain linear isomer in the gas phase.

4. Mechanism. Table 2 shows our mechanistic proposal for the formation of the $[Mo_6O_{19}]^{2-}$ anion, based on chemical intuition and on the peaks observed in the ESI-MS experiments, and supported by DFT computations. An additional mechanism is also proposed with protonated intermediates, as done previously for the formation of isopolytungstates (M2, see Supporting Information). Although collision induced dissociation (CID) very often may not access the same pathways as thermal assembly, because of both the absence of solvent and the different energy ranges sampled, we have found this to be a useful tool in understanding the assembly of POM cluster anions. The proposed mechanisms are sensible from the chemical point of view since the charge of the potential intermediates would not change significantly during the nucleation process. From a themodynamic point of view, the reaction energy for the formation of the Lindqvist molybdate from the tetrahedral monomers is less exothermic than for the corresponding tungstate (by 30 kcal mol^{-1}). This result is in agreement with the fact that the molybdate Lindqvist anions can be fragmented more easily by ESI-MS than the corresponding tungstate anions. As explained previously, the lowest-energy compact structures for each stoichiometry have been taken into account to compute the reaction energies for the different steps of the mechanism. Similar to the tungstate Lindqvist study, energetic cascade profiles are predicted for both mechanisms M1 and M2 with the last step being the most exothermic. The formation of trinuclear $[Mo_3O_{10}(OH)]^{3-}$ and pentanuclear $[Mo_5O_{16}(OH)]^{3-}$ clusters are somewhat endothermic, but are more than compensated for by the largely exothermic formation of tetramers and hexamers.

CONCLUSIONS

Using Car−Parrinello molecular dynamics to analyze the hydration-dehydration equilibrium processes for the hydrogenmolybdate anion and molybdic acid, we have confirmed that increasing the acidity of the aqueous solution involves an expansion of the coordination sphere of the Mo^{VI} ion from four to six, in agreement with experiment. Both Car−Parrinello simulations with explicit solvent molecules, and standard static DFT calculations with continuous models of solvation predict the formation of dinuclear species different from the 6c-4c structure proposed by Kepert, and also in agreement with the observed species for the polyoxotungstates.[11] Formation of dinuclear molybdates is predicted to be less favorable than tungstates. We have also found that although dichromate is a very stable species in acidic solutions, the formation of compact and closed structures with higher nuclearities is importantly endothermic, in good agreement with the low number of polyoxochromates known so far. With the help of ESI-MS experiments, we postulate mechanisms with energy-cascade profiles for the formation of the $[Mo_6O_{19}]^{2-}$ Lindqvist anion based on consecutive aggregations of hydrogenmolybdate anions followed by protonation and water condensation steps, confirming the results already observed for the isopolytungstates. Therefore, it is proposed that the $[Mo_6O_{19}]^{2-}$ anion is also formed by the aggregation of one Mo unit at a time. However, although planar Mo_3 building blocks are also found for the lowest-energy intermediate tetra- and pentanuclear species, significant differences in comparison with the isopolytungstates are detected. In general, open-chain linear structures are more favored in the case of the isopolymolybdates. The coordination sphere of the Mo^{VI} ions in polynuclear clusters might be expanded because of the interaction with the water molecules. The inclusion of the solvent effects with a continuous model provides a correct *qualitative* description of these phenomena, but explicit insertion of discrete solvent molecules is advisable whenever possible.

ASSOCIATED CONTENT

Supporting Information. Details on MS parameters and the data collection runs carried out as well as figures with representative fragmentation peaks. Tables with the computed relative energies and figures for the optimized structures analyzed in this work. Additional information about the Car−Parrinello MD and metadynamics simulations. This material is available free of charge via the Internet at http://pubs.acs.org.

AUTHOR INFORMATION

Corresponding Author

*E-mail: josepmaria.poblet@urv.cat (J.M.P.), lee.cronin@glasgow.ac.uk (L.C.), antonio.rodriguezf@urv.cat (A.R.-F.).

ACKNOWLEDGMENT

We acknowledge support from the MEC of Spain (project CTQ2008-06549-C02-01/BQU and the Ramón y Cajal Program (A.R.-F.)) and from the DGR of the Autonomous Government of Catalonia (Grants 2009SGR462 and XRQTC). H.M. would like to thank Royal Society of Edinburgh and Marie Curie actions for the financial support. L.C. wishes to acknowledge the EPSRC, The Universitiy of Glasgow, WestCHEM, the Leverhulme Trust and the Royal Society/Wolfson Foundation for a merit award.

REFERENCES

(1) (a) Pope, M. T. *Heteropoly and Isopoly Oxometalates*; Springer-Verlag: New York, 1983. (b) Long, D.-L.; Tsunashima, R.; Cronin, L. *Angew. Chem., Int. Ed.* **2010**, *49*, 1736–1758.

(2) Berzelius, J. J. *Poggend. Ann. Phys. Chem.* **1826**, *6*, 369.

(3) Müller, A.; Beckmann, E.; Bogge, H.; Schmidtmann, M.; Dress, A. *Angew. Chem., Int. Ed.* **2002**, *41*, 1162–1167.

(4) Hill, C. L., Ed.; Special issue on polyoxometalates; *Chem. Rev.* **1998**, *98*, 1.

(5) Long, D. L.; Burkholder, E.; Cronin, L. *Chem. Soc. Rev.* **2007**, *36*, 105–121.

(6) Greenwood, N. N.; Earnshaw, A. *Chemistry of the elements*; Elsevier: Oxford, 2006.

(7) Wassermann, K.; Dickman, M. H.; Pope, M. T. *Angew. Chem., Int. Ed. Engl.* **1997**, *36*, 1445–1448.

(8) (a) Bagno, A.; Bonchio, M. *Angew. Chem., Int. Ed.* **2005**, *44*, 2023–2026. (b) Duclusaud, H.; Borshch, S. A. *J. Am. Chem. Soc.* **2001**, *123*, 2825–2829. (c) Fernandez, J. A.; Lopez, X.; Bo, C.; Graaf, C.; de; Baerends, E. J.; Poblet, J. M. *J. Am. Chem. Soc.* **2007**, *129*, 12244–12253. (d) Kumar, D.; Derat, E.; Khenkin, A. M.; Neumann, R.; Shaik, S. *J. Am. Chem. Soc.* **2005**, *127*, 17712–17718. (e) Poblet, J. M.; Lopez, X.; Bo, C. *Chem. Soc. Rev.* **2003**, *32*, 297–308. (f) Quinonero, D.; Wang, Y.; Morokuma, K.; Khavrutskii, L. A.; Botar, B.; Geletii, Y. V.; Hill, C. L.; Musaev, D. G. *J. Phys. Chem. B* **2006**, *110*, 170–173. (g) Yan, L. K.; Lopez, X.; Carbo, J. J.; Sniatynsky, R.; Duncan, D. C.; Poblet, J. M. *J. Am. Chem. Soc.* **2008**, *130*, 8223–8233. (h) Wilson, E. F.; Abbas, H.; Duncombe, B. J.; Streb, C.; Long, D.-L.; Cronin, L. *J. Am. Chem. Soc.* **2008**, *130*, 13876–13884. (i) Wilson, E. F.; Miras, H. N.; Rosnes, M. H.; Cronin, L. *Angew. Chem., Int. Ed.* **2011**, *50*, 3720–3724.

(9) Kepert, D. L. *Prog. Inorg. Chem.* **1962**, *4*, 199–274.

(10) Tytko, K. H.; Glemser, O. *Adv. Inorg. Chem. Radiochem.* **1976**, *19*, 239–315.

(11) Vilà-Nadal, L.; Rodríguez-Fortea, A.; Yan, L.-K.; Wilson, E. F.; Cronin, L.; Poblet, J. M. *Angew. Chem., Int. Ed.* **2009**, *48*, 5452–5456.

(12) Filowitz, M.; Ho, R. K. C.; Klemperer, W. G.; Shum, W. *Inorg. Chem.* **1979**, *18* (1), 93–103.

(13) Cruywagen, J. J.; Heyns, J. B. B. *Polyhedron* **2000**, *19*, 907–911.

(14) Hur, N. H.; Klemperer, W. G.; Wang, R. C. *Inorg. Synth.* **1990**, *27*, 77–80.

(15) (a) *ADF 2007.01*; Department of Theoretical Chemistry, Vrije Universiteit: Amsterdam, The Netherlands, 2007. (b) Baerends, E. J.; Ellis, D. E.; Ros, P. *Chem. Phys.* **1973**, *2*, 41. (c) Versluis, L.; Ziegler, T. *J. Chem. Phys.* **1988**, *88*, 322. (d) Te Velde, G.; Baerends, E. J. *J. Comput. Phys.* **1992**, *99*, 84. (e) Fonseca Guerra, C.; Snijders, J. G.; Te Velde, G.; Baerends, E. J. *Theor. Chem. Acc.* **1998**, *99*, 391.

(16) (a) Becke, A. D. *J. Chem. Phys.* **1986**, *84*, 4524. (b) Becke, A. D. *Phys. Rev. A* **1988**, *38*, 3098–3100.

(17) (a) Perdew, J. P. *Phys. Rev. B* **1986**, *33*, 8822–8824. (b) Perdew, J. P. *Phys. Rev. B* **1986**, *34*, 7406–7406.

(18) Vosko, S. H.; Wilk, L.; Nusair, M. *Can. J. Phys.* **1980**, *58*, 1200–1211.

(19) (a) Poblet, J. M.; López, X.; Bo, C. *Chem. Soc. Rev.* **2003**, *32*, 297–308. (b) López, X.; Maestre, J. M.; Bo, C.; Poblet, J. M. *J. Am. Chem. Soc.* **2001**, *123*, 9571–9576. (c) López, X.; Fernández, J. A.; Romo, S.; Paul, J. F.; Kazansky, L.; Poblet, J. M. *J. Comput. Chem.* **2004**, *25*, 1542–1549. (d) López, X.; Miró, P.; Carbó, J. J.; Rodríguez-Fortea, A.; Bo, C.; Poblet, J. M. *Theor. Chem. Acc.* **2011**, *128*, 393–404.

(20) (a) Klamt, A.; Schüürmann, G. J. *Chem. Soc., Perkin Trans. 2.* **1993**, 799–805. (b) Andzelm, J.; Kölmel, C.; Klamt, A. *J. Chem. Phys.* **1995**, *103*, 9312–9320. (c) Klamt, A. J. *Chem. Phys.* **1995**, *99*, 2224–2235.

(21) Pye, C. C.; Ziegler, T. *Theor. Chem. Acc.* **1999**, *101*, 396–408.

(22) *CPMD*; IBM Corp.: Armonk, NY, 1990−2006; MPI für Festkörperforschung: Stuttgart, Germany, 1997−2001.

(23) (a) Troullier, N.; Martins, J. L. *Phys. Rev. B* **1991**, *43*, 1993–2006. (b) Louie, S. G.; Froyen, S.; Cohen, M. L. *Phys. Rev. B* **1982**, *26*, 1738–1742.

(24) Kachmar, A.; Bénard, M.; Rohmer, M. M.; Boero, M.; Massobrio, C. *J. Phys. Chem. A* **2009**, *113*, 9075–9079.

(25) Car, R.; Parrinello, M. *Phys. Rev. Lett.* **1985**, *55*, 2471–2474.
(26) (a) Nosé, S. *J. Chem. Phys.* **1984**, *81*, 511–519. (b) Nosé, S. *Mol. Phys.* **1984**, *52*, 255–268. (c) Hoover, W. G. *Phys. Rev. A* **1985**, *31*, 1695–1697.
(27) (a) Rodríguez-Fortea, A.; Vilà-Nadal, L.; Poblet, J. M. *Inorg. Chem.* **2008**, *47*, 7745–7750. (b) Biarnes, X.; Ardèvol, A.; Planas, A.; Rovira, C.; Laio, A.; Parrinello, M. *J. Am. Chem. Soc.* **2007**, *129*, 10686–10693. (c) Blumberger, J.; Ensing, B.; Klein, M. L. *Angew. Chem., Int. Ed.* **2006**, *45*, 2893–2897. (d) Rodríguez-Fortea, A.; Iannuzzi, M. *J. Phys. Chem. C* **2008**, *112*, 19642–19648. (e) Rodríguez-Fortea, A.; Iannuzzi, M.; Parrinello, M. *J. Phys. Chem. C* **2007**, *111*, 2251–2258. (f) Rodríguez-Fortea, M.; Iannuzzi, M.; Parrinello, M. *J. Phys. Chem. B* **2006**, *110*, 3477–3484. (g) Stirling, A.; Iannuzzi, M.; Parrinello, M.; Molnar, F.; Bernhart, V.; Luinstra, G. A. *Organometallics* **2005**, *24*, 2533–2537.
(28) (a) Laio, A.; Parrinello, M. *Proc. Natl. Acad. Sci. U.S.A.* **2002**, *99*, 12562–12566. (b) Iannuzzi, M.; Laio, A.; Parrinello, M. *Phys. Rev. Lett.* **2003**, *90*, 238302–238306. (c) Laio, A.; Rodríguez-Fortea, A.; Gervasio, F. L.; Ceccarelli, M.; Parrinello, M. *J. Phys. Chem. B* **2005**, *109*, 6714–6721.
(29) Sprik, M. *Faraday Discuss.* **1998**, *110*, 437–445.
(30) Vilà-Nadal, L.; Rodríguez-Fortea, A.; Poblet, J. M. *Eur. J. Inorg. Chem.* **2009**, 5125–5133.
(31) Fernandez, J. A.; López, X.; Poblet, J. M. *J. Mol. Catal. A* **2007**, *262*, 236–242.
(32) Walanda, D. K.; Burns, R. C.; Lawrence, G. A.; Von Nagy-Felsobuki, E. I. *J. Chem. Soc., Dalton Trans.* **1999**, 311–321.
(33) Llusar, R.; Sorribes, I.; Vicent, C. *J. Cluster Sci.* **2009**, *20*, 177–192.
(34) Tezé, A.; Hervé, G. *Inorganic Syntheses*; John Wiley and Sons: New York, 1990; Vol. 27.